ISSN 1990-7478, Biochemistry (Moscow), Supplement Series A: Membrane and Cell Biology, 2019, Vol. 13, No. 3, pp. 260–267. © Pleiades Publishing, Ltd., 2019.
Russian Text © The Author(s), 2019, published in Biologicheskie Membrany, 2019, Vol. 36, No. 4, pp. 262–270.

Microdomain Organization of Internodal Myelin

G. V. Maksimov[a, d, *], N. P. Kutuzov[b], V. V. Shutova[c], and S. N. Orlov[a]

[a] *Biology Department, Moscow Lomonosov State University, Moscow, 119892 Russia*
[b] *Faculty of Health and Medical Sciences, Department of Biomedicine, University of Copenhagen, Copenhagen, 2200 Denmark*
[c] *National Research Mordovia State University, Saransk, 430005 Russia*
[d] *Federal State Autonomous Educational Institution of Higher Education "National Research Technological University "MISIS", Moscow, 119049 Russia*
**e-mail: gmaksimov@mail.ru*

Received February 12, 2019; revised February 17, 2019; accepted February 20, 2019

Abstract—The orientation and ordering of the molecules of carotenoids and fatty acids of phospholipids in myelin of nerve fiber was investigated using Raman spectroscopy. A method for the quantitative description of the order of the molecules in myelin lipid bilayer has been developed. It was established that the difference in the distribution of the molecules of carotenoids and phospholipids is associated with the morphology of myelin and nerve fiber. The molecules of carotenoids are predominantly perpendicular to the surface of the lipid bilayer of myelin, while phospholipids are oriented at an angle of 45° to it. It is assumed that the microdomain organization of the internodal myelin is due to the presence of areas with high degree of saturation and order of the fatty acid chains of phospholipids.

Keywords: nerve fiber, myelin, Raman spectroscopy, carotenoid, phospholipid
DOI: 10.1134/S1990747819030164

INTRODUCTION

The study of changes in the structure and properties of myelin during nerve fiber excitation is an important area of molecular physiology. It is known that myelin isolates the paranodal region of the fiber, reducing its effective electrical capacity and thereby providing a higher overall rate of excitation transfer over myelinated fiber. During the excitation or activation of a number of Schwann cell (SC) receptors, not only the structure of myelin changes, but also the content of potassium and calcium ions in its compartments [1]. It was proved using electron microscopy that the structure of myelin is characterized by alternating dense (contrast) and loose layers; the period is 16–18.5 nm in peripheral nervous system (PNS) and 15–17 nm in central nervous system (CNS); the length of the internodal segment varies from 150–200 μm (in CNS) to 1 mm (in PNS) [2–4]. It was shown by scanning X-ray diffraction microscopy that myelin lamellae in the internodal area are characterized by a period of about 200 Å [2]. Probably one of the reasons of the microheterogeneity of myelin may be the different orientation of the lipid bilayers (LB) relative to each other along the nerve fiber. It is important that the packing direction of myelin lamellae is not radial [2, 4]. Structures, leading to local disorganization of myelin, are notches of Schmitt–Lanterman (NSL), which cause an irregular extension of the cytoplasm between the layers of myelin.

Raman spectroscopy (RS) makes it possible to study the vibrational energy spectra of molecules and by this means to analyze the chemical structure and conformation of the molecules [5]. RS was used to study the state of myelin lipids of nerve fibers during series of action potential [6–14]. However, when Raman spectra were recorded from different areas of myelin fibers (myelin and myelin-sheath gaps) several questions arose. For example, the size of the focal volume (the volume of space from which Raman spectra are recorded) is comparable to the size of a part of the object. In addition, the presence of carotenoids in myelin nerve fibers is not only of scientific interest [9], but also provides an opportunity to create a technology for testing the state of LB. For example, depending on the chemical structure of carotenoid molecules they can be oriented in LB in different ways: molecules of nonpolar carotenoids (beta-carotene) can be oriented both perpendicular and parallel to LB. It is important that the orientation of the carotenoid molecule can affect the order of the "tails" of fatty acids of membrane phospholipids in LB and, accordingly, the physico-chemical properties of myelin [15, 16]. In this

Abbreviations: SC, Schwann cell; LB, lipid bilayer; NSL, notches of Schmitt–Lanterman; RS, Raman spectroscopy; OPD LB, optical path difference of the light beam; FD, focal doublet; LIM, laser interference microscopy.

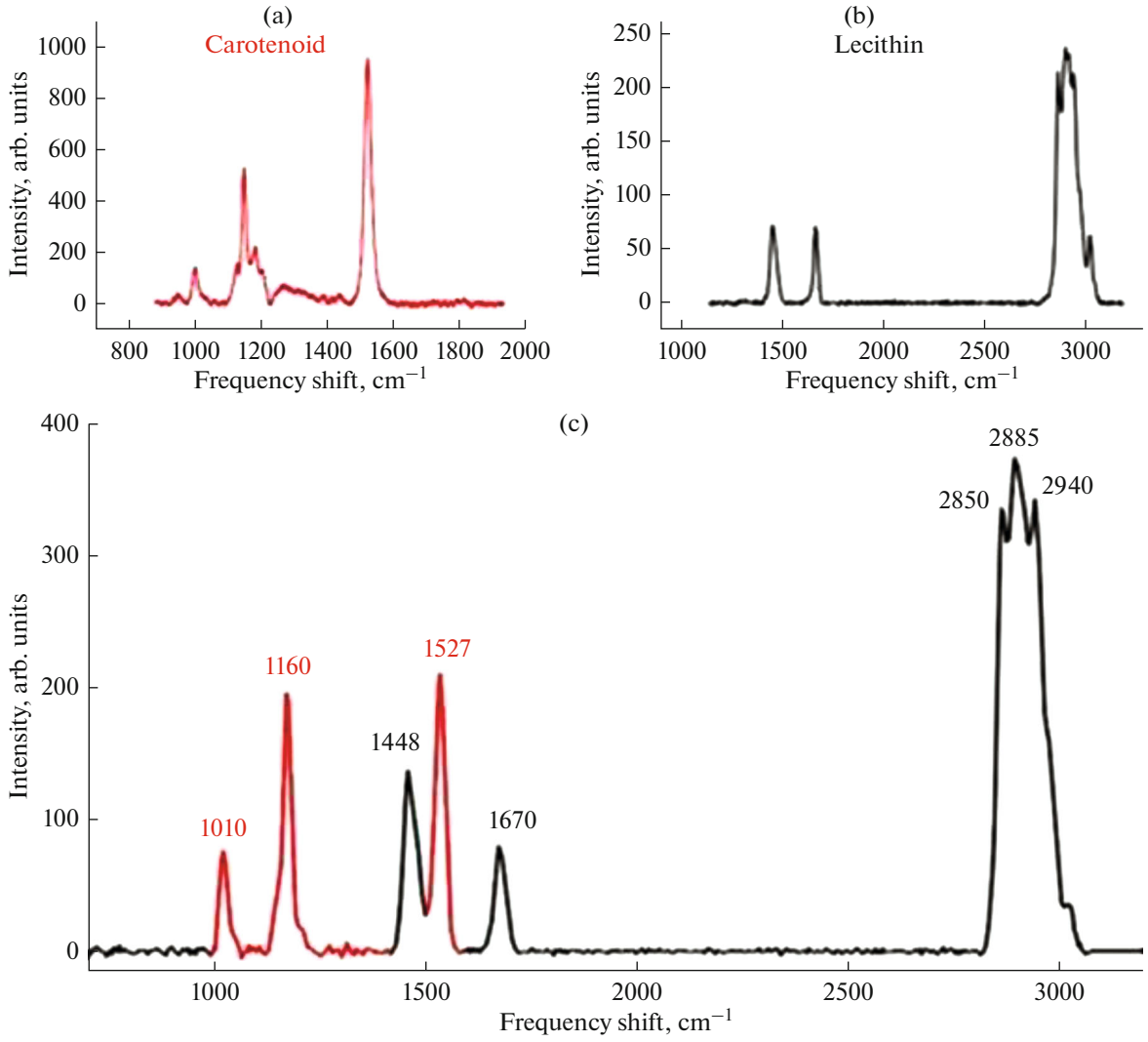

Fig. 1. Raman spectra of carotenoids (a), lecithin (b), and myelin nerve fiber (c).

regard, we used the method of polarized Raman spectroscopy (PRS) to study the orientation ordering of carotenoids and lipids [17, 18].

The aim of this work was to develop an approach for the quantitative description of the ordering of molecules in LB and to identify the microdomain organization of myelin nerve fiber.

MATERIALS AND METHODS

Objects of study. Myelin nerves of a common frog (*Rana temporaria*) served as the objects of the study. Animals were anesthetized with propofol (50 mg/kg). Single nerve fibers were placed in a plastic chamber with Ringer's solution containing NaCl (Sigma) 100 mM, KCl (Sigma) 2 mM, $CaCl_2$ (Sigma) 1.08 mM, 10 HEPES (Sigma), pH 7.4 (adjusted with NaOH), and covered with a coverglass (0.17 mm). The nerve fibers selected for the experiment contacted with the surface of the cover glass that allowed to control the angle of inclination of the object and minimize aberrations.

Raman microspectroscopy. Raman spectra were recorded using a WITec alpha–300 system with a ND:YAG continuous solid-state laser (wavelength 532 nm). Linearly polarized light was focused on the object using 20× (NA = 0.4) or 50× (NA = 0.8) lenses. The average output power of the laser from the lens was about 0.5 mW. The accumulation time of a single spectrum varied from 10 s to 2 min. To measure the anisotropy of the Raman spectra, the analyzer was placed in front of the pinhole of the microscope, which made it possible to record plane-polarized light. The RS measurements included single Raman spectra, Raman spectra recorded along a line, or two-dimensional images. The lateral and axial resolution was 1.2 and 9.7 μm for the 20× lens, and 0.9 and 7.5 μm for the 50× lens, respectively [10–14]. To identify the

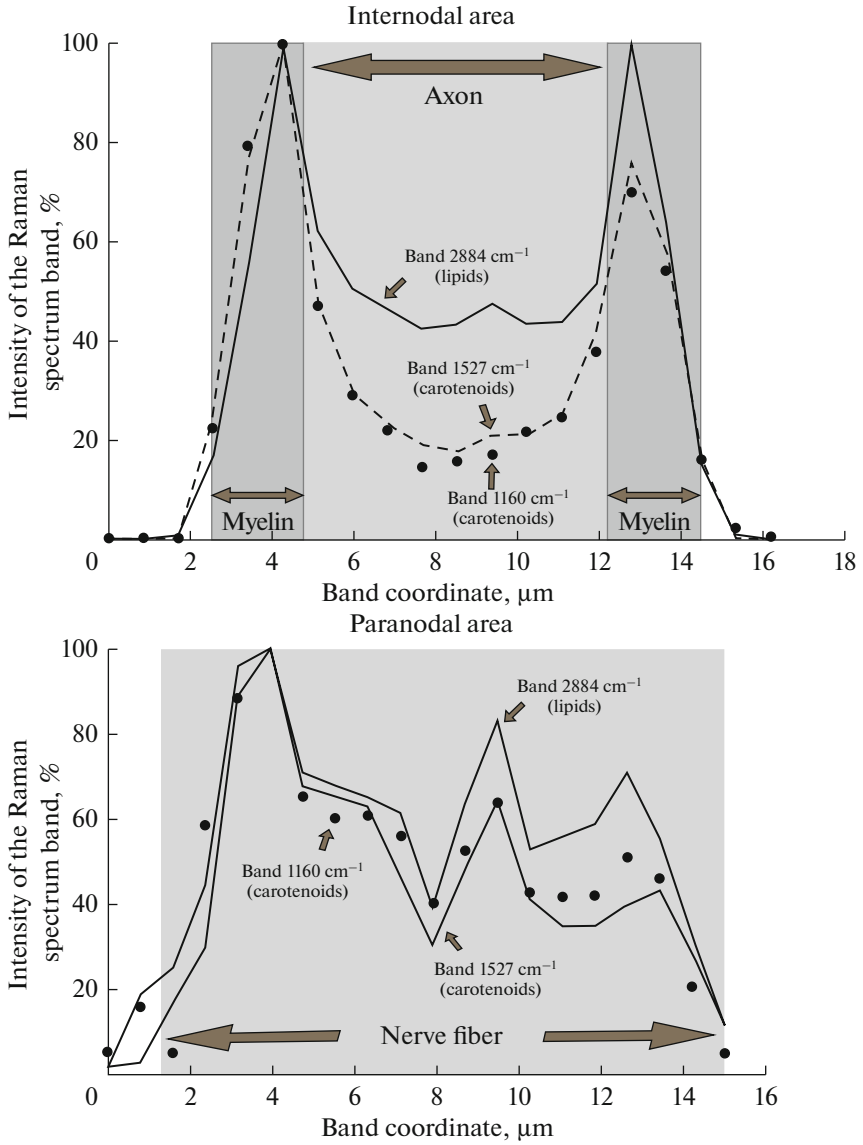

Fig. 2. The distribution of the intensities of the bands of the Raman spectrum in internodal and paranodal areas of myelin nerve fibers.

contribution of vibrations of the characteristic bonds of the molecules of carotenoid and fatty acids of the phospholipids of myelin nerve fibers, a number of ratios of the Raman spectra were used (see below). The Raman bands of myelin nerve fiber were identified using the spectra of carotenoids and lecithin [5].

Laser interference microscopy. Measurements of the optical path difference of the light beam (ODLB) were performed using an automated interference microprofilometer MIA-1 based on a MII-4 Linnik interferometer (LOMO, Russia). The objects were illuminated with unpolarized light of a LED laser with a wavelength of 650 nm and the power of 5 mW. The radiation power on the studied cell was no more than 3 mW. The image was focused using a 30× lens with a numerical aperture NA = 0.65; the image was recorded using a 12-bit VS-415U black-and-white video camera (NPK Videoscan, Russia). The resolution of the images was 512 × 512 pixels [19].

Statistical processing of the data. All obtained data were divided into two groups. The first one was the ratio of the intensities of the bands of Raman spectra; the second one was the ordering parameters $\langle P_2 \rangle$ and $\langle P_4 \rangle$. Normal distribution of sample means allowed using Student's *t*-test for comparison of mathematical expectations of two general sets corresponding to the control and experiment. Thus, the student's *t*-test with unequal variances was used to compare the ratio of the intensities of the Raman spectra bands ($p < 0.05$).

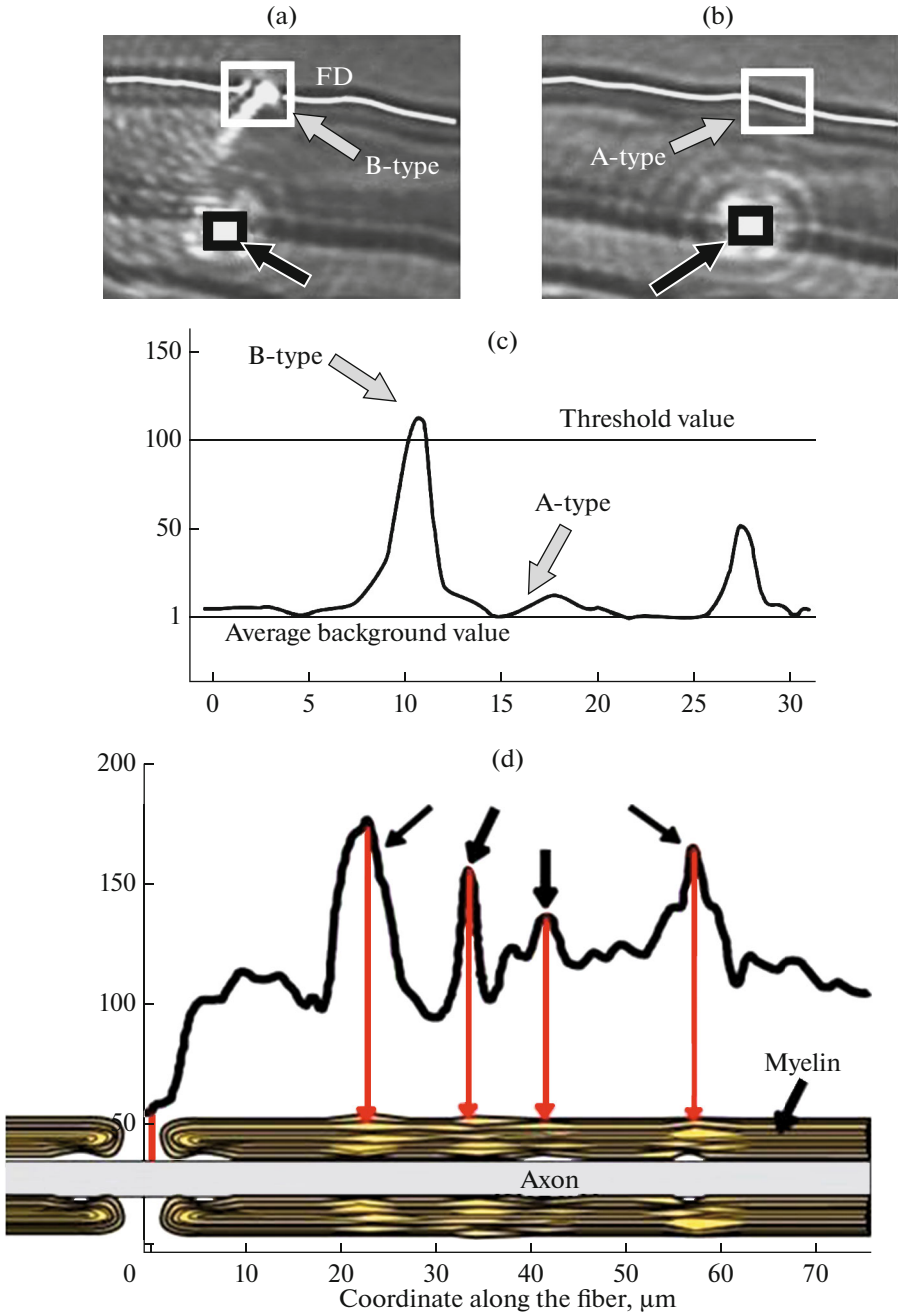

Fig. 3. Laser beam propagation in different areas of the myelin LB (a, b), intensity distribution of the focal doublet (FD) along the fiber (c), and the profile of OPD LB along the fiber (d). *Black arrows* and *black squares* indicate places of laser focus; *gray arrows* and *white squares* indicate the expected place of the FD recordings. *Ordinate* in (c) is the intensity of the band of the Raman spectrum and in (d), the value of OPD LB (both in m^{-9}); *abscissa* in (c) and (d) is the distance along the fiber, μm.

RESULTS AND DISCUSSION

It was found that the Raman spectrum of myelin nerve fiber is a superposition of the spectra of β-carotene and lecithin (Fig. 1). Scanning in the range of 900–1700 cm^{-1} revealed the bands characterizing flexural vibrations of methyl side groups $-CH_3$ in the molecules of carotenoids (1004 cm^{-1}); vibrations of –C–C– bonds of carotenoids (1160 cm^{-1}); rotational vibrations of $-CH_2-$ of the alkyl radicals in the lipids (1300 cm^{-1}); flexural vibrations of $-CH_2-$ of the alkyl radicals in the lipids (1440 cm^{-1}); vibrations of –C=C– bonds of carotenoids (1527 cm^{-1}); and vibrations of –C=C– bonds of the alkyl radicals of unsaturated fatty acids in the phospholipids (1655 cm^{-1}).

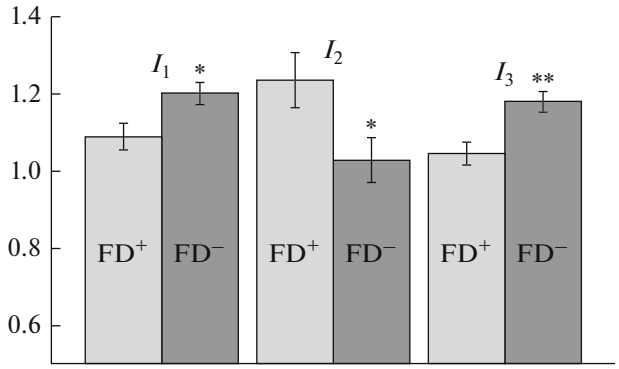

Fig. 4. Comparison of the ratios of the intensities of the major bands of the Raman spectrum for the FD^- and FD^+ types of areas. The data are presented as mean ± standard error.

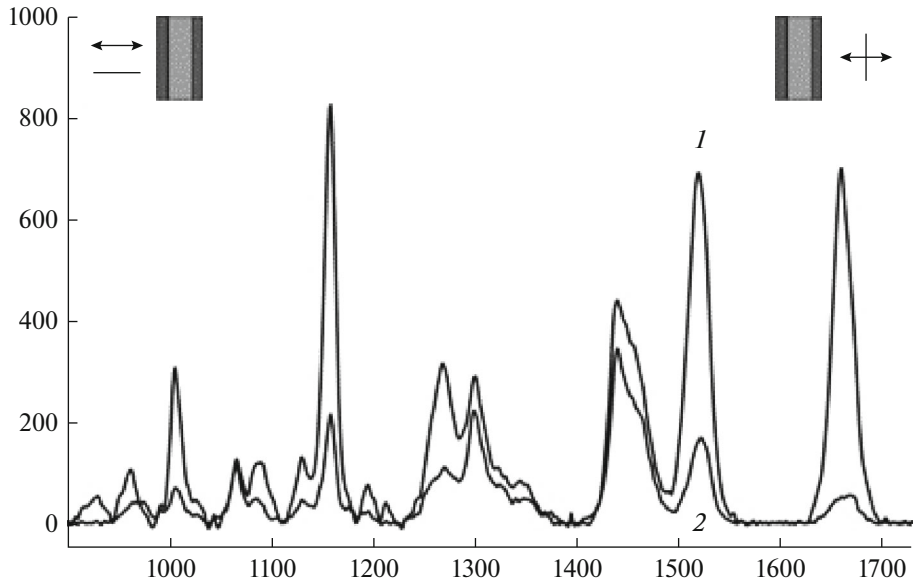

Fig. 5. Raman spectra of myelin in the region of 900–1700 cm^{-1} at different orientations of the polarizer and analyzer relative to the nerve fiber: polarizer and analyzer are parallel (*1*) or perpendicular (*2*) to each other. *Abscissa*, frequency shift, cm^{-1}; *ordinate*, intensity, arb. units.

Symmetric vibrations of the methylene groups $-CH_2-$ of the lipids (2850 cm^{-1}); asymmetric vibrations of the methylene groups $-CH_2-$ and $-CH_2-$ of the lipids (2884 – 2885 cm^{-1}); vibrations of methylene groups $-CH_2-$ and symmetric vibrations of –CH– groups of the lipids (2932–2940 cm^{-1}) were revealed in the region of 2800–3000 cm^{-1} [19, 20]. From the whole set of the above-mentioned bands, the following intensity ratios were used to analyze the state of myelin lipids (Fig. 1): (1) I_{1527}/I_{1160} ratio (conformation of carotenoids in LB) increases with increasing lipid ordering (denoted as I_1); (2) I_{1655}/I_{1440} ratio increases with increasing the degree of fatty acid unsaturation in phospholipids (denoted as I_2); (3) I_{2884}/I_{2932} ratio (conformation of the "tails" of fatty acids of phospholipids in LB) increases with increasing ordering of lipids in LB (denoted as I_3).

It was found that the Raman spectrum of the internodal region of myelin nerve fiber is symmetric relative to its center with pronounced maxima at the fiber edges (Fig. 2). The inhomogeneous distribution of the Raman intensities in the paranodal area of the fiber is due to the disordered packing in LB involved in the formation of the so-called paranodal loops, the end fragments of myelin. Note that the distribution of the intensities of the bands of the Raman spectrum of carotenoids repeats the shape of the distribution of the amplitudes of the bands of the Raman spectrum of fatty acids of phospholipids, which indicates the localization of these molecules in LB.

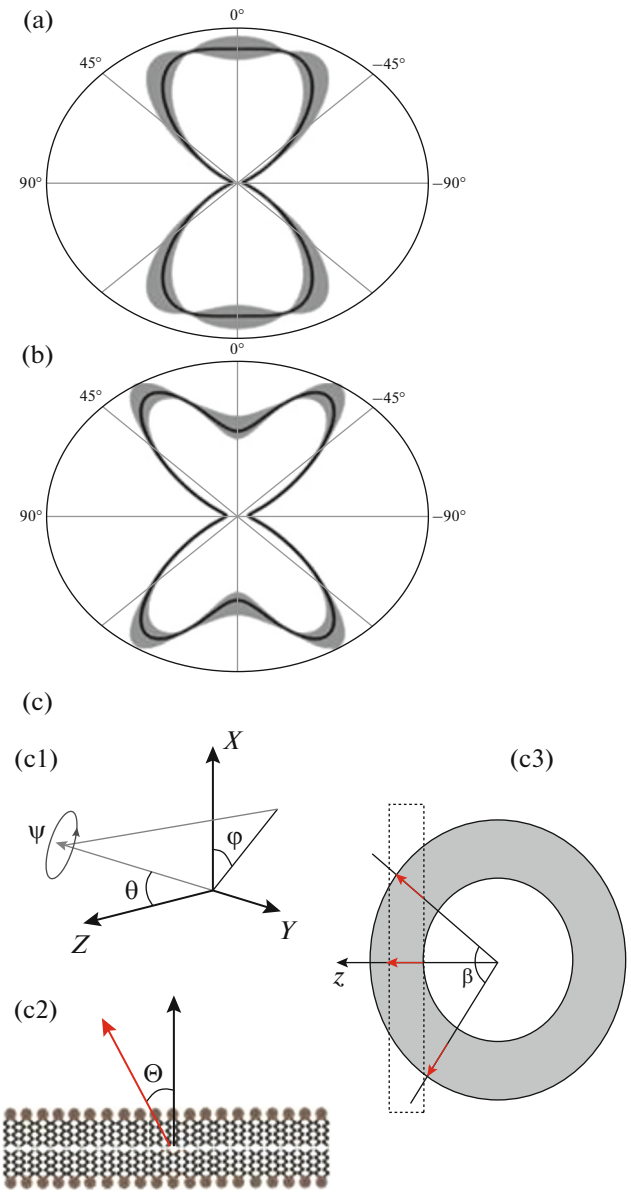

Fig. 6. Orientation distribution functions (ODF) for carotenoids (a) and phospholipids (b) of myelin. Zero angle corresponds to a direction perpendicular to the membrane. The ODF was calculated using the mean values of the ordering parameters (*solid line*). *Gray* color indicates the range of the ODF changes with varying ordering parameters within the standard error of the mean. (c) Orientation of the molecules calculated using spatial angles ((c1) and (c2)). Due to the finite curvature of myelin membranes within the focal volume (indicated by a *dotted line*), ideally oriented molecules (*arrows*) will appear to be located within angle β (c3).

During the recording of the distribution of the intensity of the focal doublet (FD), the heterogeneity in the distribution of these molecules in LB of myelin was detected: FD was absent (FD^- type) in some areas of the myelin (Fig. 3b); FD was recorded (FD^+ type) on the opposite side of the fiber in other areas of myelin (Fig. 3a). Intermediate intensity of FD was not taken into account, for example, the second maximum (Fig. 3c). Probably, the occurrence of FD is associated with the "loss" of light in myelin: if the structure of myelin was an ideal optical resonator, the light waves would circulate inside. The FD^+ type is due to the fact that at a given curvature of myelin surface, the angle of incidence of the light wave may not correspond to the angle of total internal reflection, as well as to the scattering of light on inhomogeneous myelin structures. Thus, using this approach, it is possible to study the structure of LB in different areas of myelin nerve fiber. In these experiments, the plane of polarization of the exciting laser was parallel to the axis of the nerve fiber. I_1, I_2 and I_3 were calculated from Raman spectra of carotenoids and fatty acids of phospholipids (Fig. 4). It was found that myelin membranes in the areas of the FD^+ type were characterized by a higher degree of disordering and unsaturation of the fatty acids of phospholipids. Probably, for LB with a high degree of disordered lipids, the formation of dense contacts between adjacent myelin layers is restricted as compared to more ordered membranes of the FD^- type. It is known that various local inhomogeneities, such as, for example, notches of Schmitt–Lanterman (NSL), which form the "channels" of the SC cytoplasm inside myelin, are characteristic of myelin structure. As noted earlier, the results of X-ray diffraction microscopy also indicated the presence of structural heterogeneities in myelin within the internodal area of the nerve fiber. Laser interference microscopy (LIM) was used to relate microscopic differences in the structure of LB with the density of their packaging [19]. In this series of experiments heterogeneity of the distribution of OPD LB along the nerve fiber was revealed: the minimum OPD LB corresponds to the interception of Ranvier. Thus, some properties of myelin (distribution of fatty acids by their degree of saturation and conformation of carotenoids) within the internodal region may vary.

In the study of the orientation of molecules of carotenoids and fatty acids of phospholipids of myelin, the Raman spectra of nerve fibers were recorded at different positions of the polarization plane of the laser beam relative to the fiber and a fixed polarization plane during the recording of the received signal (Fig. 5). The bands of carotenoids (1160 and 1527 cm^{-1}) and lipids (2885 cm^{-1}) of the Raman spectrum were used for calculation of the ratios of intensities $\langle J_{zz}\rangle/\langle J_{zy}\rangle$ and $\langle J_{yy}\rangle/\langle J_{yz}\rangle$ and construction of an orientation distribution function (ODF) (fraction of particles oriented with a certain angle) (Fig. 6). In the case of a symmetric bulk phase (a stretched polymer or a membrane) with molecules having cylindrical symmetry, their ODF ($N(\theta, \varphi, \psi)$) is a function of only one argument, the angle θ between the molecule axis and the normal to the membrane. Based on the Bower theory, such

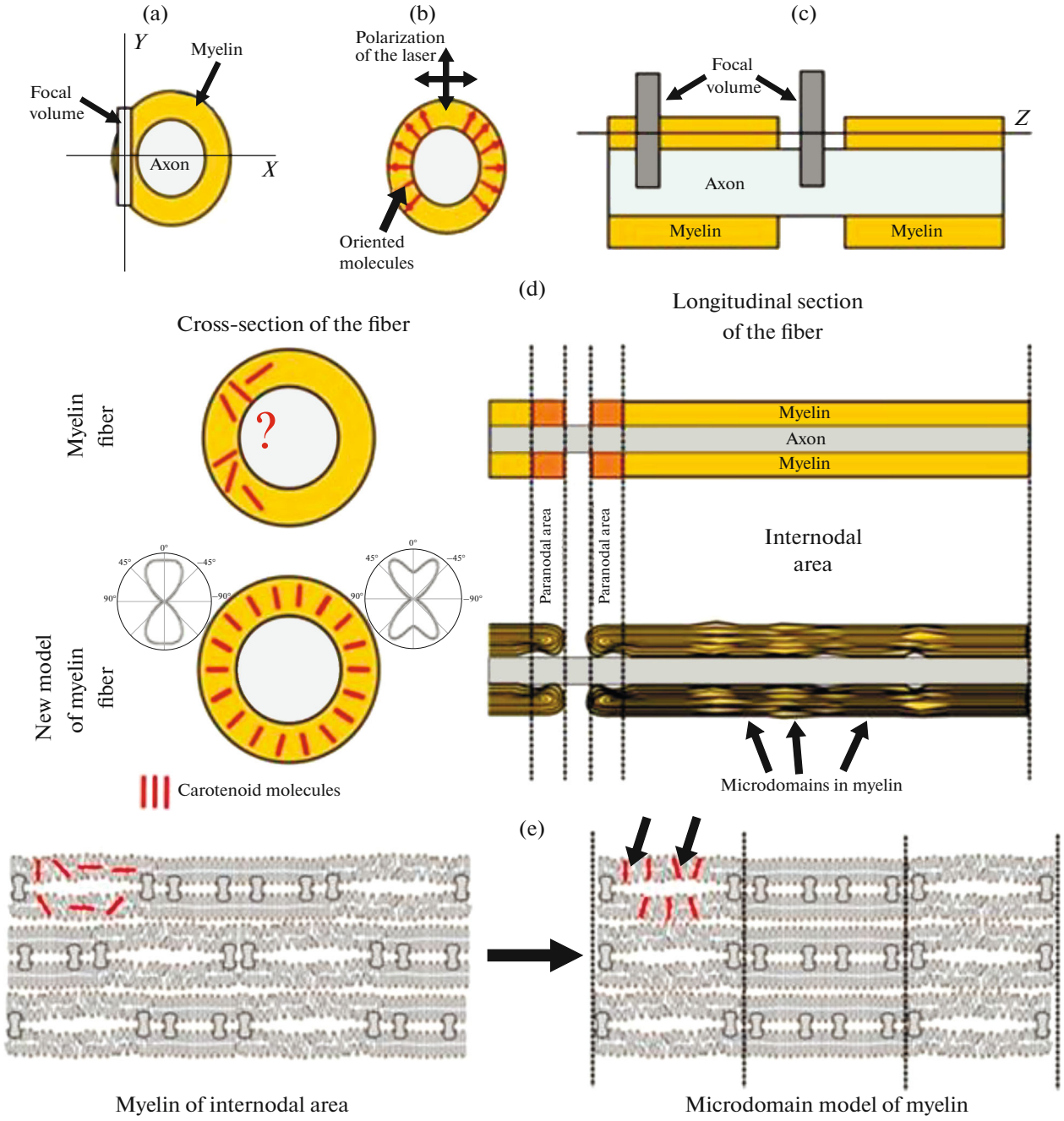

Fig. 7. Main specificities of the measurements of the Raman spectra of single nerve fibers (a–c), comments in the text. Changes in LB of the nerve fiber myelin (d). Model of the myelin structure (e).

ODF can be decomposed into a series of Legendre polynomials [20]:

$$N(\theta) = \sum_{i=0}^{\infty} \left(i + \frac{1}{2}\right) \langle P_i \rangle P_i(\cos\theta).$$

The presence of C_{2h} symmetry in carotenoid molecules allows using only even terms in the equation. By measuring Raman spectra with different positions of the polarizer and analyzer, it was possible to obtain $\langle P_2 \rangle$ and $\langle P_4 \rangle$ coefficients by solving a system of equations as described in the study of Everall et al. and use them to construct the ODF [21]. It was found that carotenoid molecules were positioned mainly perpendicular to the surface of LB, and their orientation depended on the chemical structure and composition of the membrane [16–18, 20].

Previously, only NSL were considered as inhomogeneities of myelin internodal area (Fig. 7). We found that the microdomain structure of myelin includes

radial areas of dense myelin occupying a certain area along the fiber (Fig. 7e). Such an organization of myelin structure implies a local correlation with the properties of neighboring LB of myelin. Note that, unlike NSL, such microdomains cannot be detected by standard optical microscopy; for their study it is necessary to use the visualization method we have developed.

ACKNOWLEDGMENTS

The work was supported by the Russian Science Foundation (project no. 19-79-30062).

COMPLIANCE WITH ETHICAL STANDARDS

Conflict of interests. The authors declare that they have no conflict of interest.

Statement on the welfare of animals. All procedures were performed in accordance with the European Communities Council Directive (November 24, 1986; 86/609/EEC) and the Declaration on humane treatment of animals. The Protocol of experiments was approved by the Bioethics committee of the Faculty of Biology, Lomonosov Moscow State University (no. 82-O of June 8, 2017).

REFERENCES

1. Trapp B.D., Kidd G. J. 2004. Structure of myelinated axon. In: *Myelin biology and disorders*. San Diego: Academic Press, p. 3–27.
2. Kirschner D.A., Hollingshead C.J. 1980. Processing for electron microscopy alters membrane structure and packing in myelin. *J. Ultrastructure Res.* **73** (2), 211–232.
3. Suter U., Nave K.-A. 1999. Transgenic mouse models of CMT1A and HNPP. *Ann. New York Acad. Sci.* **883** (1), 247–253.
4. Schmitt F.O., Bear R.S., Palmer K.J. 1941. X-ray diffraction studies on the structure of the nerve myelin sheath. *J. Cell. Compar. Physiol.* **18** (1), 31–42.
5. Szalontai B., Bagyinka Cs., Horvath L.I. 1977. Changes in the raman spectrum of frog sciatic nerve during action potential propagation. *Biochem. Biophys. Res. Comm.* **76** (3), 660–665.
6. Maksimov G.V., Churin A.A., Paschenko V.Z., Rubin A.B. 1990. Raman spectroscopy of the 'potential sensor' of potential-dependent channels. *Gen. Physiol. Biophys.* **9** (4), 353–360.
7. Maksimov G.V., Musuralieva G.T., Churin A.A., Pashchenko V.Z. 1989. The influence of the protein-lipid interactions in the excitable membranes on the conformation of carotenoids. *Biofizika* (Rus.). **34** (3), 420–424.
8. Maximov G.V., Churin A.A., Pashchenko V.Z., Rubin A.B. 1985. Study of the nature of regulation of potential-dependent channels by Raman spectroscopy. *Biofizika* (Rus.). **30**, (4), 620–624.
9. Verdiyan E., Bibineyshvili E., Kutuzov N., Maksimov G. 2015. Role of Schwann cell in regulation of myelin sheath properties during nerve fiber excitation and activation of purinergic receptors. *GLIA Bilbao 2015: Abstracts Oral Presentations, Posters, Indexes*. **63**, E76–E469.
10. Bulygin F.V., Dracheva O.E., Kutuzov N.P., Lyaskovskii V.L., Maksimov G.V., Nikolaev Yu A. 2014. Determination of the metrological characteristics of the near-field scanning optical microscope in the study of biological objects. *Measurement Techniques*. **56** (10), 1173–1180.
11. Sarycheva A.S., Semenova A.A., Polyakov A.Y., Kozmenkova A.Y., Grigorieva A.V., Goodilin E.A., Parshina E.Y., Brazhe N.A., Maksimov G.V. 2014. Ultrasonic-silver-rain preparation of SERS substrates. *Materials Lett*. **121**, 66–69.
12. Kutuzov N.P., Brazhe A.R., Maksimov G.V., Lyaskovskiy V.L. 2014. Orientational ordering of carotenoids in myelin membranes resolved by polarized Raman microspectroscopy. *Biophys. J.* **107** (4), 891–900.
13. Kutuzov N.P., Brazhe A.R., Lyaskovskiy V.L., Maksimov G.V. 2015. Laser beam coupling into nerve fiber myelin allows one to assess its structural membrane properties. *J. Biomed. Optics*. **20** (5), 050501.
14. Kutuzov N., Gulin A., Lyaskovskiy V., Natochenko N., Maksimov G. 2015. ATP-mediated compositional change in peripheral myelin membranes: A comparative Raman spectroscopy and time-of-flight secondary ion mass spectrometry study. *PLoS ONE*. **10** (11), e0142084.
15. van de Ven M., Kattenberg M., van Ginkel G., Levine Y.K. 1984. Study of the orientational ordering of carotenoids in lipid bilayers by resonance-Raman spectroscopy. *Biophys. J.* **45** (6), 1203–1209.
16. Mishra N.N., Liu G.Y., Yeaman M.R., Nast C.C., Proctor R.A., McKinnell J., Bayer A.S. 2011. Carotenoid-related alteration of cell membrane fluidity impacts *Staphylococcus aureus* susceptibility to host defense peptides. *Antimicrobial Agents Chemother.* **55** (2), 526–531.
17. Snyder R.G., Strauss H.L., Elliger C.A. 1982. Carbon-hydrogen stretching modes and the structure of *n*-alkyl chains. 1. Long, disordered chains. *J. Phys. Chem.* **86** (26), 5145–5150.
18. Cho Y., Kobayashi M., Tadokoro H. 1986. Raman band profiles and mobility of polymethylene chains. *J. Chem. Phys.* **84** (8), 4636–4642.
19. Berestovskaya Y.Y., Gerasimenko L.M., Yusipovich A.I., Maksimov G.V., Rubin A.B., Levin G.G., Shutova V.V. 2011. New possibilities of studying microbial objects by laser interference microscopy. *Biophysics*. **56** (6), 1063–1068.
20. Nobbs J.H., Bower D.I., Ward I.M. 1979. Comparison of polarized fluorescence with polarized raman and infrared dichroism measures of orientation in uniaxially drawn poly (ethylene terephthalate). *J. Polymer Sci. Polymer Physics Edition*. **17** (2), 259–272.
21. Everall N., Chalmers J., Mills P. 1996. Use of polarized resonance Raman spectroscopy of a polyene probe, and FT-IR dichroism, to probe amorphous-phase orientation in uniaxially drawn poly(ethylene). *Appl. Spectroscopy*. **50** (10), 1229–1234.

Translated by E. Puchkov